Ultrasonic velocity measurements on thin rock samples: experiment and numerical modeling

Alexey Yurikov[1], Maxim Lebedev[1], and Marina Pervukhina[2]

Right Running Head: Ultrasonic measurements on thin samples

[1]Curtin University, Department of Exploration Geophysics, Kensington, Western Australia.
E-mail: alexey.yurikov@postgrad.curtin.edu.au; m.lebedev@curtin.edu.au

[2]CSIRO Energy, Kensington, Western Australia. E-mail: marina.pervukhina@csiro.au

ABSTRACT

An ultrasonic pulse transmission method is a gold standard for laboratory measurements of rock elastic properties for decades and is used by oil and gas industry and service companies routinely. In spite of the wide acceptance and usage of ultrasonic pulse transmission method, experimentalists are still looking for ways to further extend the limits of its applicability and to improve its state-of-the-art practices. One of the problems that limits wider application of the method is the length of the standard samples used (~40-100 mm). This is a crucial limitation either in the case of damaged core when preparation of a standard size sample is impossible or in the case when ultrasonic experiment is combined with saturation or desiccation processes that might be extremely time-consuming on the long samples. On the other hand, thinner samples are not typically used due to implication of inhomogeneity of stress fields inside and while few results of the measurements on thin disc samples have been reported in the literature, the detailed justifications of the procedures have not been done yet. To fill this gap, we compare ultrasonic velocities measured at confining stresses up to 50 MPa done on standard and thin samples with the length of 60 mm and 15 mm, respectively. First we describe a new developed experimental setup for ultrasonic measurements on thin discs and discuss the detailed experimental procedure. Then we use finite element modeling to numerically simulate stress fields in the both types of samples. Finally, we compare the ultrasonic velocities measured on the thin discs and on standard samples and discuss how to obtain reliable elastic properties on thin samples.

INTRODUCTION

Ultrasonic Pulse Transmission (UPT) method is widely used for laboratory measurements of elastic properties of rocks (e.g., Hughes & Cross, 1951; Birch, 1960; Steward & Peselnick, 1977; Vernik and Nur, 1992; Mah and Schmitt, 2001; Prasad, 2002; Nakagawa et al., 2002; Kitamura et al., 2003; Schubnel et al., 2003; Fortin et al., 2007; Kono et al., 2009; Blake et al., 2012; Lebedev et al., 2013; Sarout et al., 2014; Bauer et al., 2016). Over decades the method was

elaborated and many challenging aspects of ultrasonic measurements have been addressed (e.g., Dellinger and Vernik, 1994; Molyneux and Schmitt, 2000; Dewhurst and Siggins, 2006). One of the major improvements of the UPT method is a possibility of velocity measurements under controlled confining and uniaxial stresses (e.g., Christensen and Wang, 1985; Scott et al., 1993; Dewhurst and Siggins, 2006; Ougier-Simonin et al., 2011). Accurate measurements of stress dependencies of rock elastic properties allowed prediction of velocity perturbations caused by stress changes related to production/injection as well as led to development of theoretical models that allowed to get an insight into the rock microstructure (e.g., Sayers and Kachanov, 1995; Saenger et al., 2006; Pervukhina et al., 2010; Pervukhina et al., 2011; De Paula et al., 2012). Accurate calibration of the time-lapse seismic responses caused by the stress changes requires establishing correct velocity stress dependencies, which implies uniform and homogeneous loading of samples during the ultrasonic experiments. The stress field in a sample depends on its size and the standards for rock samples dimensions used in UPT measurements were established in the early studies (e.g., Birch, 1960; Hughes & Cross, 1951). Birch (1960) showed that the most convenient shape for samples is cylindrical, and its length to diameter ratio should not exceed five to prevent excessive energy dissipation by wave reflections on the sample boundaries. This aspect ratio of the length to diameter of samples for ultrasonic measurements was further influenced by rock mechanics sample preparation procedure, which requires the length of the sample to be at least twice larger than the diameter to insure the uniform loading. Over the years these constraints on the length to diameter ratio became industry standards (ASTM International, 2008; ASTM International, 2014). Nowadays, typical samples used for ultrasonic measurements are cylinders with 20-50 mm diameter and 40-100 mm length. Hereafter, we refer to such samples as standard samples.

Ultrasonic velocity measurements are often performed on samples subjected to desiccation and saturation/resaturation of the samples with different fluids. Such experiments might be extremely time-consuming if done on samples of 40-100 mm length. For example, the

desiccation process can take several months to stabilize saturation of low permeability samples of standard size (e.g., Ferrari et al., 2014). Thinner samples are preferable for such studies. Ultrasonic velocity measurements are often combined with other measurements fulfilled on the same rock samples. For instance, comprehensive characterization of rock samples usually comprises dielectric permittivity measurements that are used to quantify water content (Garrouch and Sharma, 1994; Jones and Friedman, 2000; Josh et al., 2012). Thin disc samples 10-15 mm long are required for such experiments (Josh, 2014). Moreover, often researchers have to work with limited core material or brittle rocks, when manufacturing of standard samples is challenging.

In spite of these three obvious reasons to cut down the length of samples used for ultrasonic velocity measurements, namely, economy of rock material, shorter saturation/desiccation time and compatibility with other experimental setups, just a few measurements on shorter samples were reported (for instance, Fujii and Kawashima 1995; Kitamura et al., 2003; Kono et al., 2009). One of the possible reasons of limited use of short samples is the implication of an inhomogeneous stress distribution in such samples. However, the issue of stress distribution inside tested samples should be addressed for each experimental setup like it is done for geomechanical experiments in, for instance, Yoshikawa and Mogi, (1990), Raper and Erbach (1990), Özcan et al. (2009), Saksala et al. (2013). Saenger et al. (2014) applied finite element method (FEM) modeling to check homogeneity of stress distribution inside standard cylindrical samples used for low frequency measurements.

In this study, we compare ultrasonic velocity measurements done on standard plugs (38 mm diameter, 60 mm length) and thin discs (38 mm diameter, 15 mm length). In first section, we describe a newly developed experimental setup for UPT measurements on thin discs and compare the results of experimental measurements on standard and thin disc samples of selected set of rocks and materials. Then in section Numerical modeling we explain the FEM modeling of the experimental rig. Finally, we discuss how the geometry of the experimental rig

influence the results of UPT measurements and show how to obtain reliable elastic properties of rocks from measurements on thin disc samples.

EXPERIMENTAL SETUP AND SAMPLES

To investigate the feasibility of UPT measurements on thin disc samples and to benchmark the obtained experimental results on the measurements done on standard plugs, the standard cylindrical samples with 60 mm length and 38 mm diameter are prepared from poly-methyl methacrylate (PMMA), dry Berea sandstone, dry Bentheim sandstone, and preserved Opalinus shale samples (see Figure 1). The thin disc of 15 mm length is cut off from each standard sample after its ultrasonic velocities are measured. By this we try to minimize the effect of heterogeneity in natural samples.

To obtain ultrasonic P- and S-wave velocities, we use two-transducer pulse transmission technique. The schematic of the experimental equipment arrangement is presented in Figure 2. A rectangular form electrical Pulser/Receiver 5077PR (Olympus, Ltd.) and Digital Phosphor Oscilloscope TDS 3034C (Tektronix, Ltd.) are used to generate and acquire electrical signals. A pair of piezoelectric shear transducers V153 1MHz/.5″ (Olympus Panametrics-NDT™) is used as a source and a receiver of ultrasonic pulses. Both shear and compressional waves are generated by such transducers as was demonstrated previously, e.g. Lebedev et al. (2013). All electronic components are synchronized in time and the dead time of electronics as well as the dead time of transducers are taken into account by calibration of the system.

A sample is placed inside a rubber sleeve (38.5 mm inner diameter) in the Hoek cell between two polyether ether ketone (PEEK) pistons. The measurements are done under a hydrostatic stress in a range from 2 to 50 MPa. The axial stress is applied to cylindrical samples by a hydraulic actuator mounted at the top of the experimental rig, whereas radial stress is applied directly to jacketed sample via pressurized hydraulic oil (Figure 2). Among the

delivering axial stress to samples inside the Hoek cell, the PEEK pistons are used to separate P- and S-wave arrivals in time and to ensure planar wavefront when the pulse reaches tested samples (Lebedev et al., 2013). We use two pairs of PEEK pistons (short and long) for standard and thin disc samples, respectively, thus we perform the experiment with two different setups as shown in Figure 2. The length to diameter ratio of both setups does not exceed five so Birch's condition (Birch, 1960) is met.

Typical records of waveforms are shown in the Figure 3. As reported in Lebedev et al. (2013), the travel time of P-wave can be determined as the moment of the first onset of energy, while the travel time of S-wave corresponds to the moment of high magnitude signal arrival. In order to ensure a consistent approach and to enhance precision of travel times picking, we apply algorithms of automatic picking described, for example, by Akram and Eaton (2016). We use iterative crosscorrelation-based workflow for waves arrival time picking (De Meersman et al., 2009) applied for a set of waveforms obtained for the same sample under different applied pressures. The initial time picks required for the workflow are selected using STA/LTA (short and long time average) ratio method (Trnkoczy et al., 2002) in time windows localized in the neighborhood of P- or S-wave arrivals. This workflow is applied independently for P- and S-wave travel time detection.

Implementing of the described workflow is feasible due to using of PEEK pistons in the experimental setup, as arrivals of P- and S-waves are separated in time by more than 50 μs, S-wave signal is less contaminated with multiple oscillations, and it is possible to locate time windows for STA/LTA algorithm of sufficient width capturing only P- or only S-wave. Elastic properties of PEEK pistons are stress dependent, thus aluminum samples (15 and 60 mm long) placed instead of measurement samples are used for calibration of the travel times of both P- and S-waves in PEEK cylinders in the pressure range 2-50 MPa. This calibration also includes the dead time of the electronics.

ULTRASONIC VELOCITIES IN STANDARD SAMPLES AND THIN DISCS

The velocities measured on standard and thin samples as functions of hydrostatic confining stresses within the range of 2-50 MPa are shown in Figure 4. Solid markers and dots with error bars represent the velocities measured on standard plugs and thin discs, respectively. The measurements are done without pore pressure control and, consequently, the confining stresses are equal to the effective ones.

The experimental errors are shown only for measurements on thin discs, as they are approximately four times higher than the ones for velocities measured on standard plugs. As the elastic wave velocities are calculated as $V = L/T$, where L is the length of the sample and T is the measured travel time, the errors of velocity measurements are inversely proportional to the lengths of samples:

$$\Delta V = \sqrt{\left(\frac{\partial V}{\partial L}\Delta L\right)^2 + \left(\frac{\partial V}{\partial T}\Delta T\right)^2} = \sqrt{\left(\frac{V}{L}\Delta L\right)^2 + \left(\frac{V^2}{L}\Delta T\right)^2} = \frac{V}{L}\sqrt{(\Delta L)^2 + (V\Delta T)^2}. \quad (1)$$

Here ΔL and ΔT are absolute errors of sample length measurements and travel times measurements respectively. Using thin 15 mm disc sample leads to increase of the experimental errors in four times. However, using systematic approach of automatic picking of travel times described earlier, we exclude human factor influence on the experimental errors and enhance accuracy of measurements.

As expected, the velocities measured on the PMMA samples show little stress dependency. At the same time, the velocities measured on Berea and Bentheim sandstones show typical for sandstones exponential saturation into a linear trend at low applied pressures (e.g., Christensen and Wang, 1985). This strong stress sensitivity is explained with the closure of cracks and grain contacts with the increase of applied pressure (e.g., Walsh, 1965; Shapiro, 2003; Pervukhina et al., 2010). Compared to sandstones, Opalinus shale shows only slight increase of

V_p and V_s propagating and polarized along the bedding plane with the increase of confining stress, which is typical for shales with preserved saturation (e.g., Dewhurst and Siggins, 2006).

The velocities measured on discs and standard samples are within the experimental errors, however, the differences are higher in sandstones, which show the highest stress sensitivity in the sample collection. In the next section, we simulate stress distribution in Berea and Bentheim sandstones to better understand the differences in stress distribution in the thin and standard stress-sensitive sandstones.

NUMERICAL MODELING

The numerical simulations are fulfilled using Abaqus Finite Element Analysis software (Dassault Systèmes) to understand the influence of the experimental setup and sample geometry on a stress field in tested samples and to compare stress distribution inside standard and thin samples. We build two 3D models imitating the experimental setups with standard (Figure 5a) and disc (Figure 5b) samples placed in a Hoek cell between pair of short and long PEEK pistons, respectively. We numerically apply pressure to the setup in the same way as it is done in the experiment: 1) the radial pressure P_{radial} is applied in a region where the rubber sleeve in a Hoek cell confines the sample and PEEK pistons (S_r at Figure 5); 2) the axial pressure P_{axial} is applied at the top surface of the setups in a region where the top transducer jacket attached to the upper PEEK piston (S_a^{top} at Figure 5).

As the area on top of the upper PEEK piston, where the axial pressure is applied, differs from the area of the contact between the piston and a sample, the magnitude of axial pressure acting on a sample P_{axial}^{sample} is not the same as the magnitude of P_{axial} applied to the top surface S_a^{top}. The force F produced by the pressure applied to the upper PEEK piston through the area S_a^{top} is transmitted to the sample acting on different area of the base of a cylinder sample S_{base}:

$$F = P_{axial} S_a^{top} = P_{axial}^{sample} S_{base}. \quad (2)$$

In order to apply hydrostatic pressure to the sample inside the Hoek cell ($P_{axial}^{sample} = P_{radial}$), the magnitude of the numerically applied axial pressure should correspond to the magnitude of applied radial pressure as the ratio of the area of the base of a cylinder sample, S_{base}, to the area of surface S_a^{top}:

$$P_{axial} = \frac{S_{base}}{S_a^{top}} P_{axial}^{sample} = \frac{S_{base}}{S_a^{top}} P_{radial}. \quad (3)$$

At the bottom surface (S_a^{bot}) the nodes of the model are restricted to move in vertical direction imitating the contact between bottom PEEK pistons and the transducer jacket. The contacts between PEEK pistons and samples are assumed to be perfect, i.e. there is no slip or friction between these parts.

To analyze stress field in standard and disc samples within the described geometries we use Abaqus Standard solver and calculate components of stress tensor within the model spatial cells. The hexahedral cells with ~1mm length in vertical direction is used (Figure 5c).

We numerically apply to the samples hydrostatic pressure in a range 2-50 MPa as we have done during the experiment. The stress dependent elastic properties of PEEK pistons are taken into account in the model, namely, Young's modulus, *E*, and Poisson's ratio, ν, are calculated from experimentally measured velocities in PEEK (Table 1). Assuming the velocities measured on the standard samples to be the reference data, we derive stress-dependent *E* and ν of Berea and Bentheim sandstones from experiment on standard plugs (Table 1) and assign these elastic properties to both standard and thin samples within the numerical models. Generally, the dynamic moduli used for simulation in this work differ from the static moduli. However, here we

focus on comparison of stress distribution inside the samples of different geometry, thus the demonstrated results are valid as long as the tested samples are assigned the same properties.

The simulated stress distribution inside the setups with standard and thin Berea sandstone samples under isotropic confining stress of 50 MPa is shown in Figure 6 color-coded by $p = -1/3 \cdot \mathrm{tr}(\boldsymbol{\sigma})$, an independent of the coordinate system first invariant of the stress tensor $\boldsymbol{\sigma}$. Figure 6c shows rescaled stress distribution in the thin disc and the standard sample in order to better visualize a detailed stress distribution inside the samples. One can observe non-uniform distribution of p inside the standard and thin samples, which is caused by edge effects, i.e. concentration of stress at the edges, also leading to a well-known barrel shape of a loaded cylindrical sample (Charlez, 1991). The asymmetry of the stress field inside the samples is caused by geometry of the pistons, which have different sizes in the model as well as in the experiment.

As the elastic waves travel are initiated and registered by the transducers of certain size mounted at the top and bottom of the setups, we select the central parts of the samples shown in Figure 6c with dashed line for analysis of stress field. The selected parts have the diameter equal to the size of the transducers. We average the numerically simulated stress magnitude in this volume and calculate standard deviation.

In the case of the standard sample high stress areas are located primarily at the top and bottom surfaces of the cylinder near the edges. The central part of the sample is loaded uniformly, as the average stress is equal to 50.65 MPa with standard deviation of 0.86 MPa. The average magnitude of p at this volume is close to the applied confining stress of 50 MPa. Hence, the measured ultrasonic velocities are the velocities of the wave propagated throughout the medium uniformly loaded to the applied confining stress.

In the case of the thin disc sample the geometry of the setup influences the stress distribution significantly. The stress distribution is the central part of the sample is uniform, but due to the small size of the sample, the edge effects impact the central part, where stress (average stress is 55.39 MPa with standard deviation of 0.27 MPa) is ~11% higher than applied confining stress. Therefore, elastic waves propagating through the thin sample actually travel through a material under the higher stress than the confining stress applied to the setup. The described issue should be taken into account as the difference in the stress distribution in the standard and thin disc samples can result in a discrepancy of the measured velocities especially in the samples with high stress sensitivity.

To introduce a relevant correction to the stress-dependent velocities of Berea and Bentheim sandstones measured on thin discs, we calculate the average stress in the central part of the samples at applied pressures in the range 2-50 MPa. The results of the stress averaging reported in Table 2 are obtained for standard and disc Berea and Bentheim sandstones (as well as for Berea sandstone samples of intermediate sizes, which is discussed below). As mentioned before, the stress distribution along the main axis of standard samples both for Berea and Bentheim sandstones is homogeneous and close to the applied pressure with the relative differences below 1.4% and 0.6% respectively (see Figure 7). The stresses in the middle of the thin disc samples differ from the ones in the standard plugs. The relative difference for Berea sandstone sample is as high as 11% and it is almost constant for all the applied pressures. In Bentheim sandstone the relative error increases from 1.5% to 8% when pressure increases from 2 MPa to 50 MPa.

Taking into account the calculated stress distributions we apply correction to the experimental data shown in Figure 4. This correction results in shifting the data points of velocities measured on thin discs along the horizontal axis to calculated stress values (Figure 8).

DISCUSSION

The presented results raise several questions: (1) the effect of discrepancy between applied pressure and stress inside thin samples on measured elastic waves velocities, (2) the effect of length of samples on stress distribution, (3) the effect of using different materials in the setups on stress distribution.

The data reported in Table 2 show that discrepancy between applied and resultant stress inside thin disc sample could be significant (for example, up to 11% in case of Berea sandstone). However, comparing results reported in Figure 8 shows that the difference between initial and corrected data is almost negligible. The difference of 11% between the applied pressure and experienced stress is substantial only at high pressures, where in the case of this sandstone the velocity – stress curve exhibit linear trend. At pressures lower than 20 MPa, where stress dependency of velocities is significant, the stress correction in thin samples is small.

However, some rocks exhibit significant stress dependency like, for instance, Wasterly granite and Navajo sandstone from Coyner (1984) and Mavko and Jizba (1991). Therefore the accurate simulation of stress distribution is required to interpret the results of ultrasonic measurements under stress and to estimate experimental errors caused by redistribution of stress in thin samples. The geometry of an experimental setup, and, in particular, the length of the tested samples should be taken into account as a possible source of discrepancy in measured velocities.

In order to understand the effect of length of samples on stress distribution we conducted a set of numerical simulations with Berea sandstone samples of different lengths. Figure 9 shows the stress distribution inside the samples with applied isotropic confining pressure of 50 MPa. The stress distribution becomes more inhomogeneous with the stronger edge effects on the central part of the sample with the decrease of sample length. Table 2 reports the averaged stress inside the central part of samples of different lengths showing increase of discrepancy between

the applied confining stress and gained magnitude of averaged stress with the decrease of sample length (see also Figure 7).

An alternative approach to reduce the discrepancy of the measured elastic properties due to inhomogeneous stress distribution resulted from the edge effect is using a lubricant between PEEK pistons and the samples. The lubrication reduces friction and allows slip between the parts of the experimental setup resulting in more homogeneous stress field inside the samples. However, this approach has a significant drawback as a lubrication of the contacts makes the detection of the S-wave using UPT method impossible.

The material of the pistons used in the experimental rig also affects the stress distribution within samples. In our experimental rig we use the pistons made from PEEK, which is soft material with stress-dependent elastic properties. The stress-dependency of its elastic properties introduces complexity of experimental data processing, as the calibration is required for each stress state. This is one of the reasons why the pistons in the experimental rigs are traditionally made from aluminum. In order to estimate the influence of aluminum pistons on the stress distribution within the samples, we repeated the numerical modeling described in the previous section, but replaced PEEK pistons with aluminum ones.

The results (Figure 10) show that using the material with higher contrast of elastic properties compared to those of a tested sample leads to more inhomogeneous stress distribution. The average stress in the central part of the standard Berea sample is 45.73 MPa, which is significantly lower than applied stress of 50 MPa. The stress distribution is also significantly more inhomogeneous within the sample, which is shown by significant standard deviation of 4.74 MPa. In case of the thin disc of Berea sandstone, the average stress in the central part is 36.05 MPa with standard deviation of 0.99 MPa. Here, the stress field can be considered homogeneous as standard deviation is less than 3% of average stress, however the magnitude of p in the central area is significantly lower than applied 50 MPa, and the high magnitude stress

~55 MPa is concentrated at the lateral surface of the thin sample. The significant stress field inhomogeneity inside both standard and thin samples is caused by using of aluminum pistons, which elastic properties substantially differs from the elastic properties of Berea sandstone. Therefore, use of aluminum pistons instead of PEEK pistons results in simplification of calibration routine, but lead to two major drawbacks: 1) high reflection coefficient at the contact between pistons and sample resulting in low energy transmission, 2) more inhomogeneous stress distribution inside rock samples leading to inaccurate velocities measurements especially in soft stress-sensitive samples. Generally, the best option would be to manufacture pistons of a material with elastic properties similar to tested samples. However, as the results of numerical modeling show, use of different materials leads to different stress distribution inside tested samples. Thus, the UPT laboratory experiments need to be complemented with the numerical modeling to ensure the uniform stress distribution in the sample.

Finally, it is worth mentioning that the discrepancies in measured velocities between the standard samples and short discs in natural samples can be caused by inhomogeneity of the samples apart from the reasons discussed above. When a good quality core material is sufficient, desiccation/saturation processes are not time-consuming and the ultrasonic measurements are not a part of a comprehensive study that require measurements on short discs, the velocities measured on standard samples are more accurate and less affected with local heterogeneities intrinsic for natural rocks. However, in the case if the ultrasonic measurements for some reasons must be fulfilled on think discs, the reliable results can be obtained if the measurements are complemented with numerical simulation of the stress distribution within the samples.

CONCLUSION

An experimental setup for UPT measurements on thin 15 mm disc samples has been developed and compressional and shear velocities have been measured on thin and standard samples of PMMA, Opalinus shale, dry Berea and dry Bentheim sandstones. The measurements

done under confining stress in a range 2-50 MPa show that the obtained results agree within the experimental error and reliable stress dependencies are obtained on the thin disc samples as well as on the standard plugs.

At the same time, numerical modeling shows that the stress distributions in the standard samples and thin discs are different and the average stress in the thin samples between the ultrasonic transducers might deviate significantly from the applied confining stress. This fact can affect the measured ultrasonic velocities especially in soft stress-sensitive samples. We have demonstrated that, for example, in case of the thin Berea sandstone sample, the stress inside the central part of the sample along propagation of elastic waves is 11% higher than the applied confining stress. In this case the velocities measured at an applied confining stress actually correspond and have to be attributed to a higher stress. The actual stress distribution within the samples depends on the length of the sample, its elastic properties as well as elastic properties of the pistons used in the experimental setup. In the case of aluminum pistons, the relative difference between the applied confining and real stress in the sample can be significant even for samples of the standard length. Therefore, the inhomogeneity of stress field is a critical issue, which has to be taken into account during UPT measurements on rock samples. The measured velocities can be attributed to the correct stress and reliable stress dependencies can be obtained on the thin discs as well as on the standard samples if experimental measurements are combined with a numerical simulation of stress field in a given experimental setup.

ACKNOWLEDGMENTS

This work was partially funded by Curtin Reservoir Geophysical Consortium (CRGC). Alexey Yurikov was supported by Curtin Strategic International Postgraduate Research Scholarship and Australian Government Research Training Program Scholarship.

REFERENCES

Akram, J., and D. W. Eaton, 2016, A review and appraisal of arrival-time picking methods for downhole microseismic data: Geophysics, **81**, no. 5, KS67-KS87.

ASTM International, 2008, D 2845 – 08 Standard Test Method for Laboratory Determination of Pulse Velocities and Ultrasonic Elastic Constants of Rock. Retrieved from http://www.astm.org/Standards/D2845.htm

ASTM International, 2014, D 7012 – 14 Standard Test Methods forCompressive Strength and Elastic Moduli of Intact Rock Core Specimens under Varying States of Stress and Temperatures. Retrieved from http://www.astm.org/Standards/D7012.htm

Bauer, A., M. H. Bhuiyan, E. Fjær, R. M. Holt, S. Lozovyi, M. Pohl, and D. Szewczyk, 2016, Frequency-dependent wave velocities in sediments and sedimentary rocks/ Laboratory measurements and evidences: The Leading Edge, June 2016, 490-494.

Birch, F., 1960, The velocity of compressional waves in rocks to 10 kilobars, part1: Journal of Geophysical Research, **65**, 1083-1102.

Blake, O. O., D. R. Faulkner, and A. Rietbrock, 2012, The effect of varying damage history in crystalline rocks on the P- and S-wave velocity under hydrostatic confining pressure: Pure and Applied Geophysics, **170**, 493–505.

Charlez, P. A., 1991, Rock Mechaniks: Theoretical Fundamentals, Volume 1: Èditions Technip, p. 163.

Christensen, N. I., and H. F. Wang, 1985, The influence of pore pressure and confining pressure on dynamic elastic properties of Berea sandstone: Geophysics, **50**, no. 2, 207-213.

Coyner, K. B., 1984, Effects of stress, pore pressure, and pore fluids on bulk strain, velocity, and permeability in rocks: Ph.D. thesis, Massachusetts Inst. Tech.

De Paula, O., M. Pervukhina, D. Makarynska, and B. Gurevich, 2012, Modeling squirt dispersion and attenuation in fluid-saturated rocks using pressure dependency of dry ultrasonic velocities: Geophysics, **77**, no. 3, WA157-WA168.

Dellinger, J., and L. Vernik, 1994, Short Note Do traveltimes in pulse-transmission experiments yield anisotropic group or phase velocities?: Geophysics, **59**, no. 11, 1774-1779.

De Meersman, K., M. Kendall, and M. Van der Baan, 2009, The 1998 Valhall microseismic data set: An integrated study of relocated sources, seismic multiplets, and S-wave splitting: Geophysics, **74**, no. 5, B183–B195.

Dewhurst, D. N., and A. F. Siggins, 2006, Impact of fabric, microcracks and stress field on shale anisotropy: Geophysical Journal International, **165**, no. 1, 135-148.

Ferrari, A., V. Favero, P. Marchall, and L. Laloui, 2014, Experimental analysis of the water retention behaviour of shales: International Journal of Rock Mechanics & Mining Sciences, **72**, 61–70.

Fortin, J., Y. Guéguen, and A. Schubnel, 2007, Effects of pore collapse and grain crushing on ultrasonic velocities and V_p/V_s: Journal of Geophysical Research, **112**, B08207, 1-16.

Fujji, I., and K. Kawashima, 1995, Digital measurement of ultrasonic velocity: Review of Progress in Quontitative Nondestructive Evaluation, **14**, 203-209.

Garrouch, A. A, and M. M. Sharma, 1994, The influence of clay content, salinity, stress, and wettability on the dielectric properties of brine-saturated rocks: 10 Hz to 10 MHz: Geophysics, **59**, no. 6, 909-917.

Hughes, D. S., and J. H. Cross, 1951, Elastic wave velocities at high pressures and temperatures: Geophysics, **16**, 577-593.

Jones, S. B., and S. P. Friedman, 2000, Particle shape effects on the effective permittivity of anisotropic or isotropic media consisting of aligned or randomly oriented ellipsoidal particles: Water Resources Research, **36**, no. 10, 2821-2833.

Josh, M., L. Esteban, C. Delle Piane, J. Sarout, D. N. Dewhurst, and M. B. Clennell, 2012, Laboratory characterisation of shale properties: Journal of Petroleum Science and Engineering, **88–89**, 107–124.

Josh, M., 2014, Dielectric permittivity: a petrophysical parameter for shales: Petrophysics, **55**, no. 4, 319-332.

Kitamura, K., M. Ishikawa, and M. Arima, 2003, Petrological model of the northern Izu–Bonin–Mariana arc crust: constraints from high-pressure measurements of elastic wave velocities of the Tanzawa plutonic rocks, central Japan: Tectonophysics, **371**, 213–221.

Kono, Y., M. Ishikawa, M. Harigane, K. Michibayashi, and M. Arima, 2009, P- and S-wave velocities of the lowermost crustal rocks from the Kohistan arc: Implications for seismic Moho discontinuity attributed to abundant garnet: Tectonophysics, **467**, 44–54.

Lebedev, M., M. Pervukhina, V. Mikhaltsevitch, T. Dance, O. Bilenko, and B. Gurevich, 2013, An experimental study of acoustic responses on the injection of supercritical CO2 into sandstones from the Otway Basin: Geophysics, **78**, no. 4, D293–D306.

Mah, M., and D. R. Schmitt, 2001, Experimental determination of the elastic coefficients of an orthorhombic material: Geophysics, **66**, no. 4, 1217-1225.

Mavko, G., and D. Jizba, 1991, Estimating grain-scale fluid effects on velocity dispersion in rocks: Geophysics, **56**, 1940–1949.

Molyneux, J. B., and D. R. Schmitt, 2000, Compressional-wave velocities in attenuating media: A laboratory physical model study: Geophysics, **65**, no. 4, 1162-1167.

Nakagawa, S., K. T. Nihei, and L. R. Myer, 2002, Elastic wave propagation along a set of parallel fractures: Geophysical Research Letters, **29**, no. 16, 31-1 – 31-4.

Ougier-Simonin, A., Y. Guéguen, J. Fortin, A. Schubnel, and F. Bouyer, 2011, Permeability and elastic properties of cracked glass under pressure: Journal of Geophysical Research, **116**, B07203, 1-12.

Özcan, D. M., A. Bayraktar, A. Sßahin, T. Haktanir, T. Türker, 2009, Experimental and finite element analysis on the steel fiber-reinforced concrete (SFRC) beams ultimate behavior: Construction and Building Materials, **23**, 1064–1077.

Pervukhina, M., B. Gurevich, D. N. Dewhurst, and A. F. Siggins, 2010, Applicability of velocity-stress relationships based on the dual porosity concept to isotropic porous rocks: Geophysical Journal International, **181**, no. 3, 1473-1479.

Pervukhina, M., B. Gurevich, P. Golodoniuc, and D. N. Dewhurst, 2011, Parameterization of elastic stress sensitivity in shales: Geophysics **76**, 147-155.

Prasad, M., 2002, Acoustic measurements in unconsolidated sands at low effective pressure and overpressure detection: Geophysics, **67**, no. 2, 405-412.

Raper, R. L., and D. C. Erbach, 1990, Prediction of soil stresses using the finite element method: Transactions of the ASAE, **33**, no.3, 725-730.

Saenger, E. H., O. S. Krüger, and S. A. Shapiro, 2006, Effective elastic properties of fractured rocks: Dynamic vs. static considerations: International Journal of Fracture **139**, no. 3-4, 569-576.

Saenger, E. H., C. Madonna, M. Frehner, and B. S. G. Almqvist, 2014, Numerical Support of Laboratory Experiments: Attenuation and Velocity Estimations: Acta Geophysica, **62**, no. 1, 1-11.

Saksala, T., M. Hokka, V.-T. Kuokkala, J. Mäkinen, 2013, Numerical modeling and experimentation of dynamic Brazilian disc test on Kuru granite: International Journal of Rock Mechanics & Mining Sciences, **59**, 128–138.

Sarout, J., L. Esteban, C. Delle Piane, B. Maney, and D. N. Dewhurst, 2014, Elastic anisotropy of Opalinus Clay under variable saturation and triaxial stress: Geophysical Journal International, **198**, 1662-1682.

Sayers, C. M., and M. Kachanov, 1995, Microcrack-induced elastic wave anisotropy of brittle rocks: Journal of Geophysical Research, **100**, no. B3, 4149-4156.

Scott, T. E., Q. Ma, and J.-C. Roegiers, 1993, Acoustic velocity changes during shear enhanced compaction of sandstone: International Journal of Rock Mechanics and Mining Sciences, **30**, no. 7, 763-769.

Shapiro, S. A., 2003, Elastic piezosensitivity of porous and fractured rocks: Geophysics, **68**, no. 2, 482–486.

Schubnel, A., O. Nishizawa, K. Masuda, X. J. Lei, Z. Xue, and Y. Guéguen, 2003, Velocity Measurements and Crack Density Determination During Wet Triaxial Experiments on Oshima and Toki Granites: Pure Applied Geophysics, **160**, 869-887.

Steward, R., and L. Peselnick, 1977, Velocity of compressional waves in dry Franciscan rocks to 8 kbar and 300°C: Journal of Geophysical Research, **82**, 2027-2039.

Trnkoczy, A., 2002, Understanding and parameter setting of STA/LTA trigger algorithm, *in* P. Bormann, ed., New manual of seismological observatory practice: Deutsches GeoForschungsZentrum GFZ, 1-20.

Vernik, L., and A. Nur, 1992, Ultrasonic velocity and anisotropy of hydrocarbon source rocks: Geophysics, **57**, no. 5, 727-735.

Walsh, J. B., 1965, The effect of cracks on the compressibility of rocks: Journal of Geophysical Research, **70**, no. 2, 381-389.

Yoshikawa, S., and K. Mogi, 1990, Experimental studies on the effect of stress history on acoustic emission activity – A possibility for estimation of rock stress: Journal of Acoustic Emission, **8**, 113-123.

LIST OF FIGURES

Figure 1. PMMA, Berea sandstone, Bentheim sandstone, and Opalinus shale samples. Standard samples, 60 mm long, were used for experimental measurements first, than thin disc samples 15 mm long were cut out of the standard plugs. Opalinus shale sample shown in the figure is before cutting.

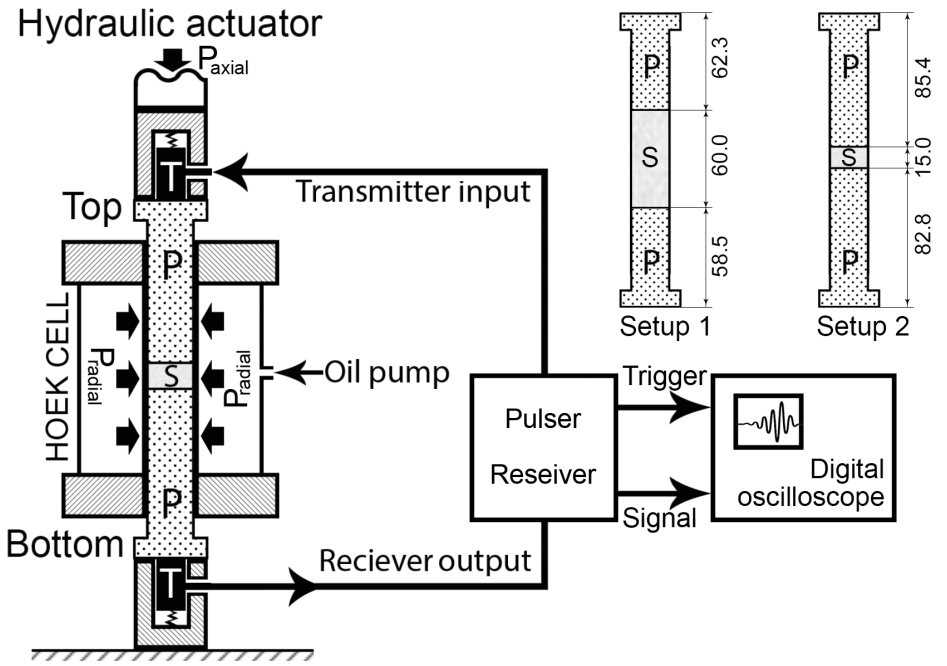

Figure 2. Schematic of the experimental equipment arrangement. T – transducer, P – PEEK piston, S – sample. Setup 1 and Setup 2 at the top right corner show standard and thin disc samples, respectively, placed between short and long PEEK pistons.

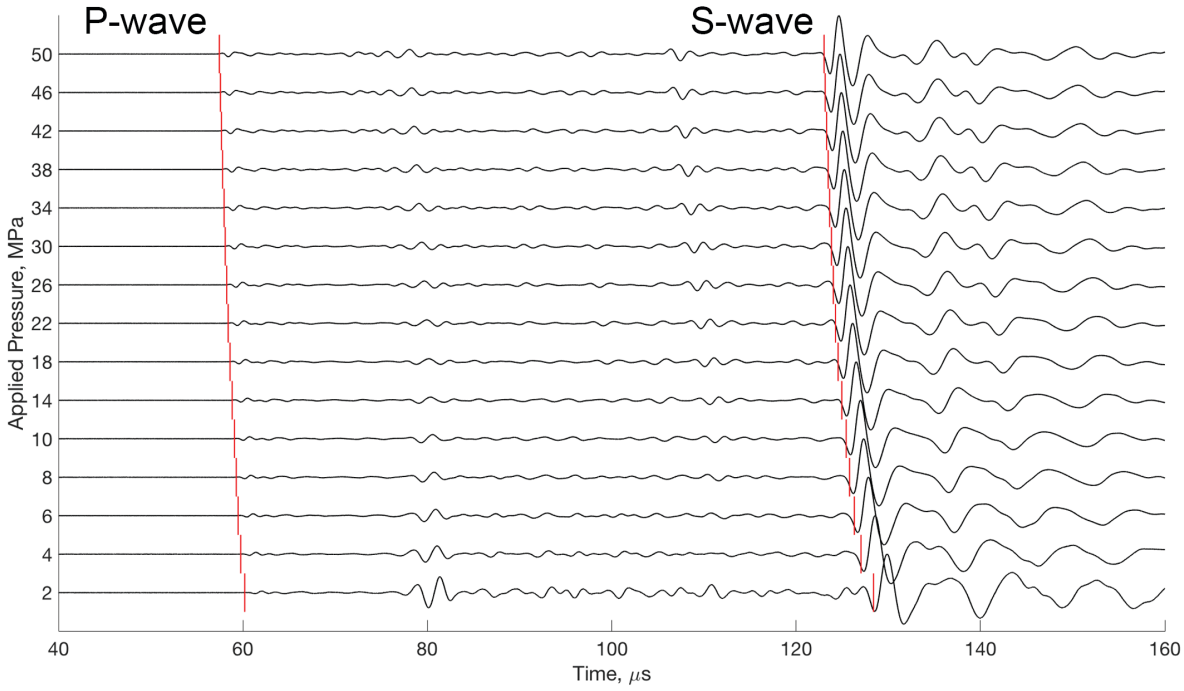

Figure 3. The example of experimentally obtained waveforms on a setup with standard dry Berea sandstone. Red vertical lines show determined arrivals of P- and S-wave.

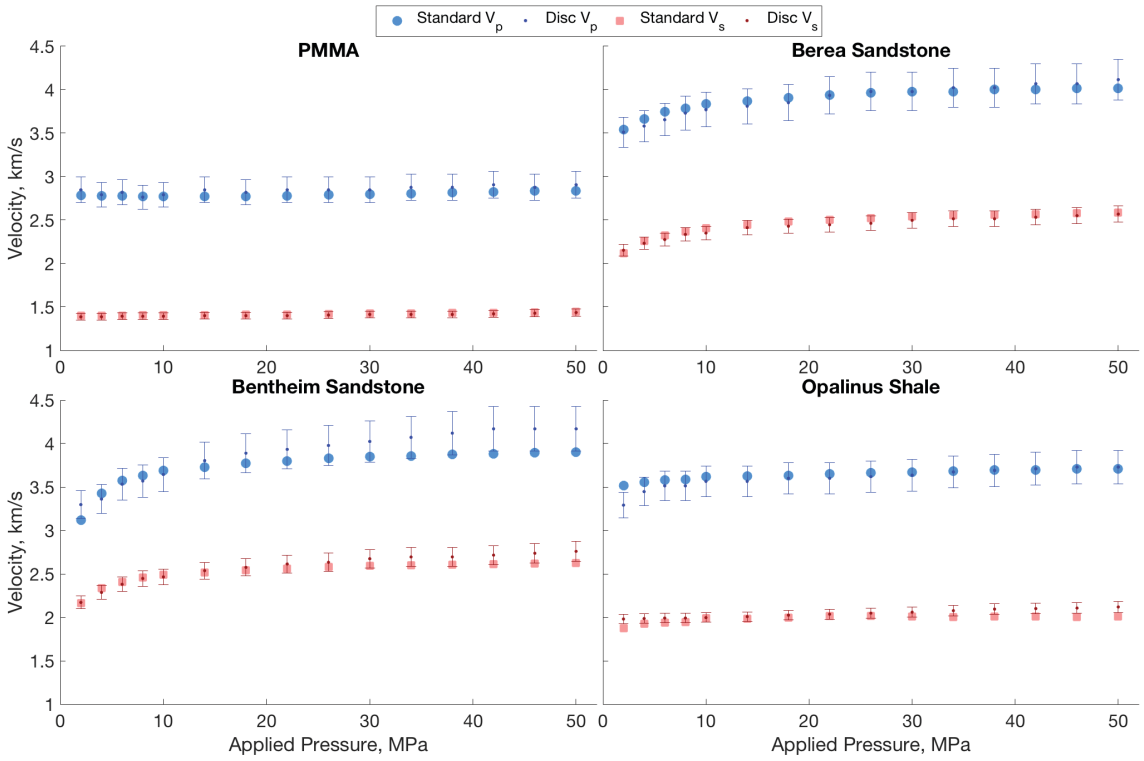

Figure 4. Measured V_p and V_s on the set of standard and thin samples made of four different materials. Experimental errors are shown for measurements on thin samples. Shear velocity V_s on the Opalinus shale is the velocity of shear wave propagating and polarized in the bedding plane direction.

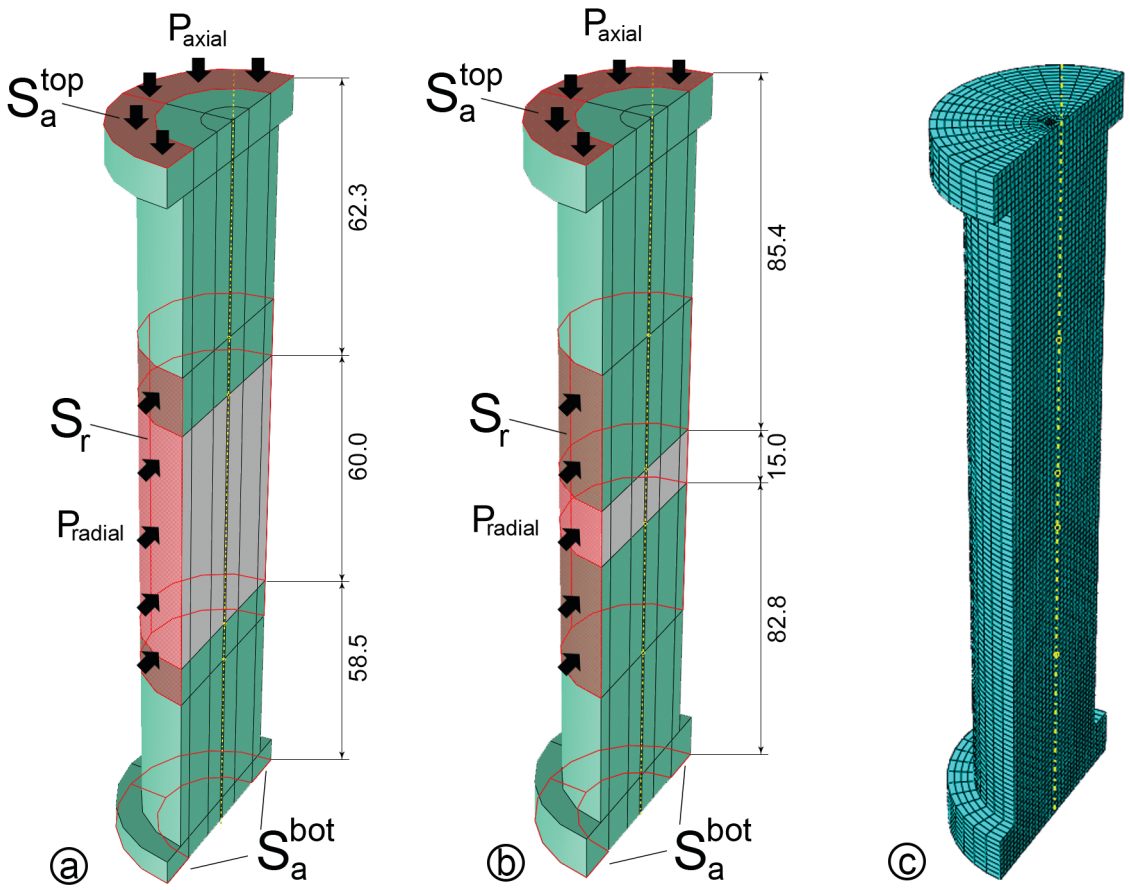

Figure 5. Abaqus model built for static stress distribution modeling. The models are full 3D copies of the experimental setups. Figure shows half of the models cut by vertical plane along the main axis. PEEK pistons are green; tested samples are gray. The areas with applied boundary conditions are highlighted with red colour. S_a^{top} – area, where axial stress P_{axial} is applied; S_r – area, where radial stress P_{radial} is applied; S_a^{bot} – fixed area, where motion of particles in vertical direction is restricted simulating rigid surface underneath the setup. All dimensions are shown in millimetres. a) The setup with standard sample; b) the setup with thin sample; c) hexahedral meshing of the models.

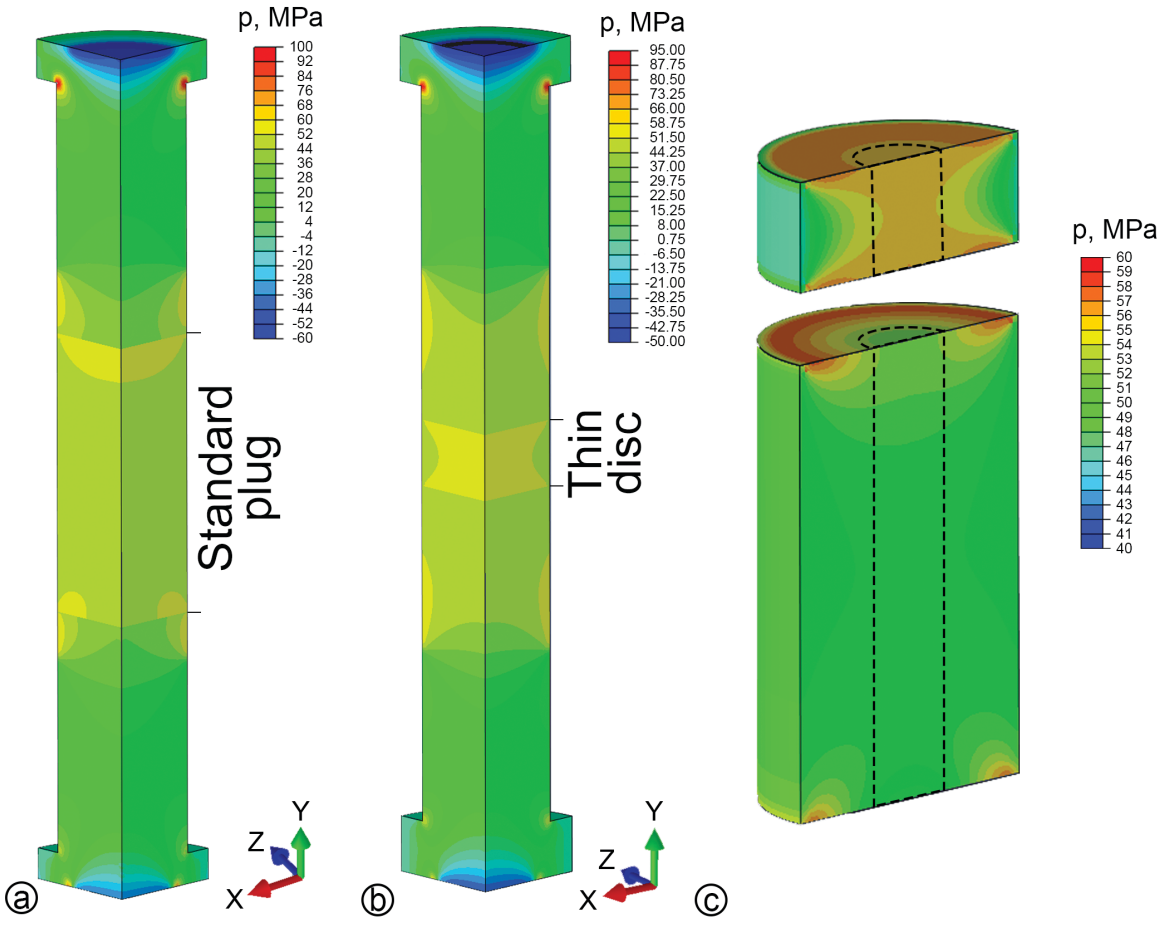

Figure 6. Modeling of static stress distribution inside the experimental setups. Applied hydrostatic pressure is equal to 50 MPa. Equivalent pressure stress $p = -(\sigma_{11}+\sigma_{22}+\sigma_{33})/3$ is colorcoded, σ_{11}, σ_{22}, σ_{33} – diagonal components of the stress tensor. a) The setup with standard Berea sandstone sample. b) The setup with thin Berea sandstone sample. c) Rescaled stress fields inside the thin and standard samples.

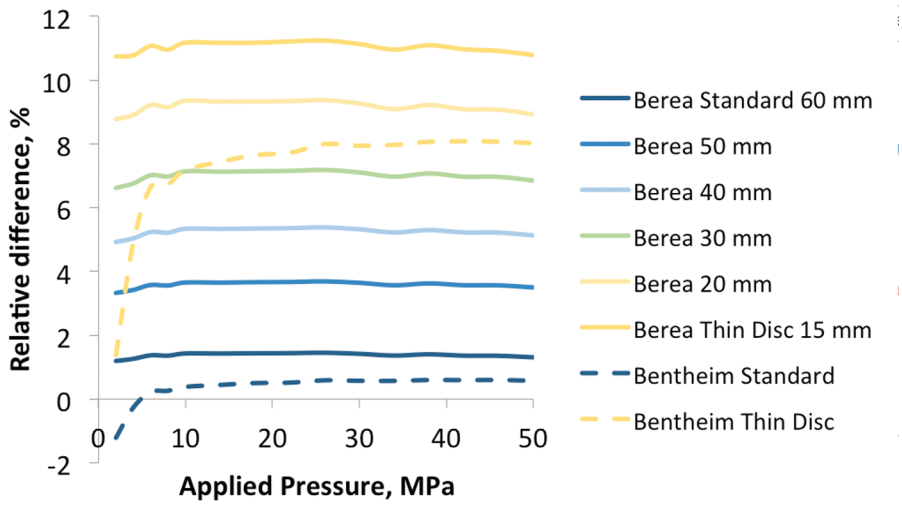

Figure 7. Relative difference between applied pressure and averaged stress in a central part of the samples, calculated from data reported in Table 2.

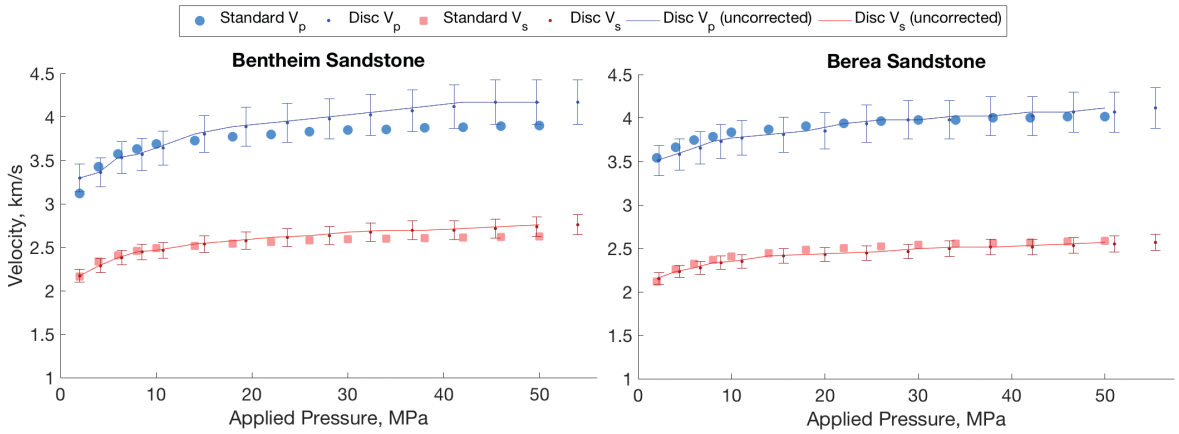

Figure 8. V_p and V_s measured on the standard Berea and Bentheim sandstone samples versus corrected V_p and V_s obtained on thin samples. Experimental errors are shown for measurements on thin samples. Solid lines represent velocities measured on thin disc samples before introduced correction.

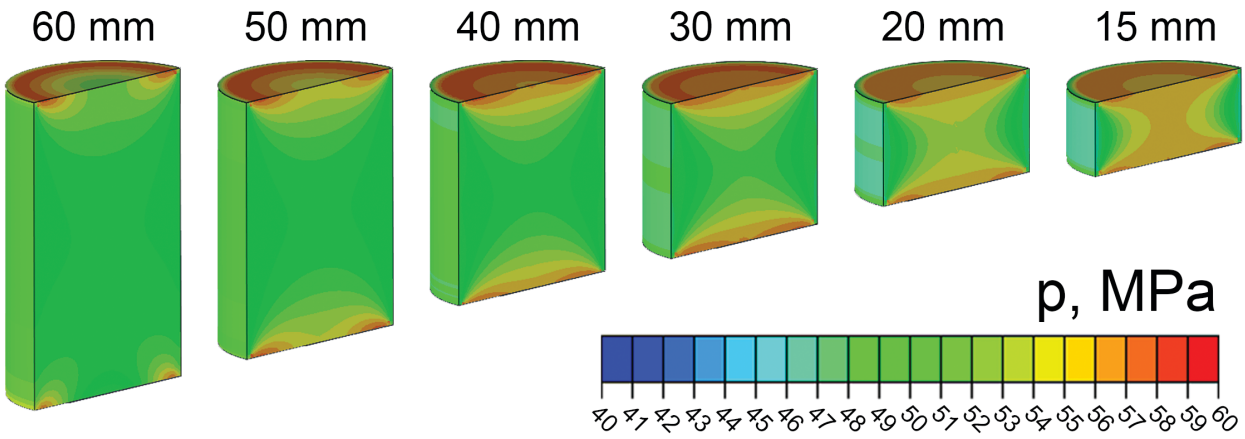

Figure 9. Results of numerical modeling of stress redistribution inside Berea sandstone samples of different lengths. Equivalent pressure stress $p = -(\sigma_{11}+\sigma_{22}+\sigma_{33})/3$ is colorcoded, σ_{11}, σ_{22}, σ_{33} – diagonal components of the stress tensor.

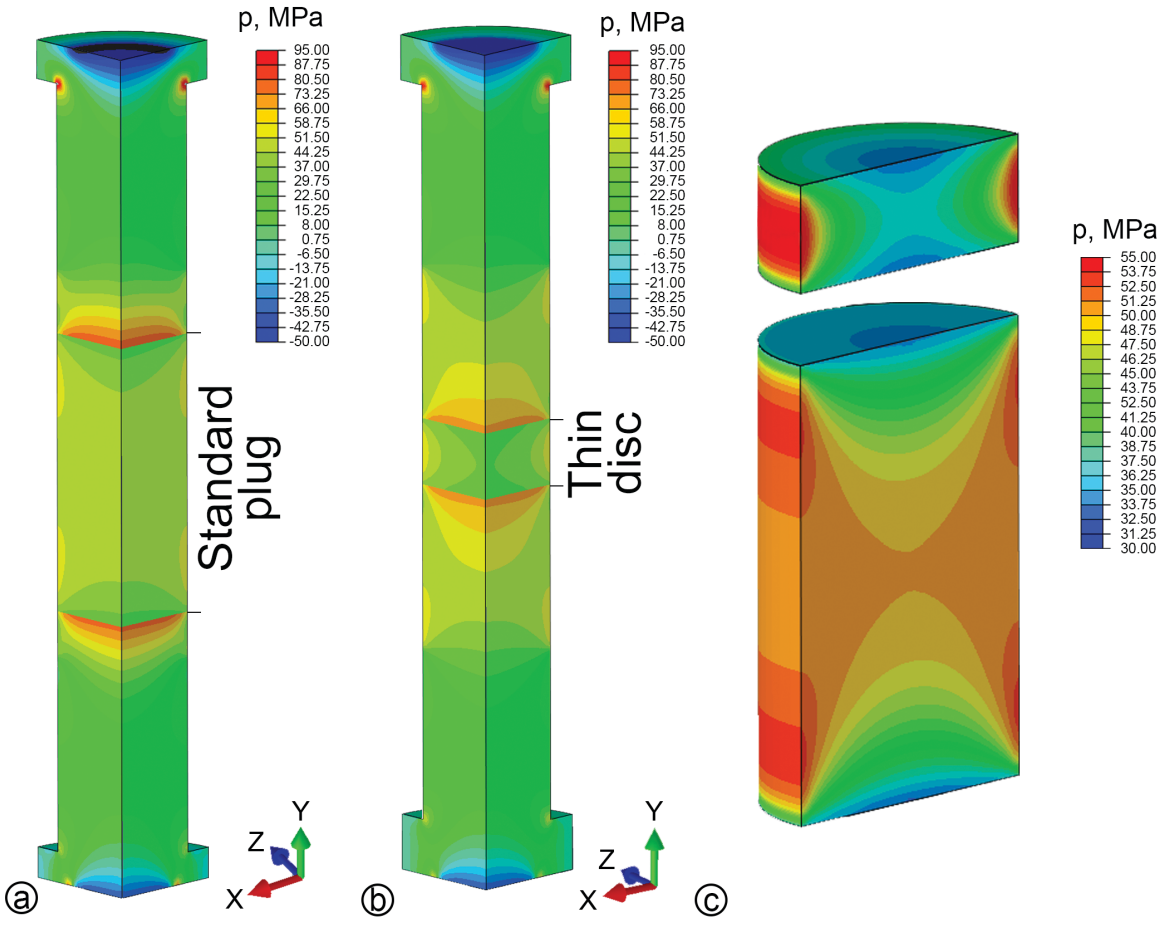

Figure 10. Modeling of static stress distribution inside the experimental setups with aluminum pistons instead of PEEK parts. Applied hydrostatic pressure is equal to 50 MPa. Equivalent pressure stress $p = -(\sigma_{11}+\sigma_{22}+\sigma_{33})/3$ is colorcoded, σ_{11}, σ_{22}, σ_{33} – diagonal components of the stress tensor. a) The setup with standard Berea sandstone sample. b) The setup with thin Berea sandstone sample. c) Rescaled stress fields inside the thin and standard samples.

LIST OF TABLES

Table 1. Stress-dependent rocks and materials properties used for modeling.

Pressure, MPa	PEEK long		PEEK short		Berea		Bentheim	
	E, GPa	ν	E, GPa	ν	E, GPa	ν	E, GPa	ν
2	4.71	0.379	4.70	0.377	23.11	0.222	19.19	0.033
4	4.71	0.379	4.71	0.378	25.63	0.195	22.99	0.062
6	4.72	0.378	4.72	0.378	27.01	0.187	24.91	0.085
8	4.73	0.379	4.72	0.378	27.86	0.177	25.75	0.077
10	4.74	0.379	4.73	0.378	28.63	0.175	26.52	0.080
14	4.76	0.379	4.74	0.379	29.41	0.168	27.10	0.081
18	4.77	0.379	4.75	0.379	30.14	0.163	27.71	0.082
22	4.78	0.380	4.76	0.379	30.60	0.161	28.10	0.080
26	4.79	0.380	4.77	0.380	31.08	0.159	28.56	0.085
30	4.80	0.381	4.78	0.380	31.38	0.155	28.85	0.082
34	4.81	0.381	4.79	0.380	31.52	0.150	28.97	0.083
38	4.82	0.381	4.80	0.381	31.87	0.153	29.22	0.086
42	4.83	0.382	4.81	0.381	31.94	0.150	29.34	0.087
46	4.84	0.382	4.82	0.381	32.19	0.149	29.46	0.088
50	4.85	0.383	4.83	0.382	32.25	0.146	29.61	0.087

Table 2. Results of numerical modeling of stress redistribution in Bentheim and Berea sandstone samples of different length. Stress values are in MPa. Standard samples are 60 mm long, thin samples are 15 mm long.

Applied pressure	Bentheim Standard	Bentheim Thin	Berea Standard	Berea 50mm	Berea 40mm	Berea 30mm	Berea 20mm	Berea Thin
2	1.98	2.03	2.02	2.07	2.10	2.13	2.18	2.21
4	3.99	4.20	4.05	4.14	4.20	4.27	4.36	4.43
6	6.01	6.40	6.08	6.21	6.31	6.42	6.55	6.66
8	8.02	8.54	8.11	8.28	8.42	8.56	8.73	8.88
10	10.04	10.72	10.14	10.37	10.53	10.71	10.94	11.12
14	14.06	15.04	14.20	14.51	14.75	15.00	15.31	15.56
18	18.09	19.38	18.26	18.66	18.96	19.29	19.68	20.01
22	22.11	23.70	22.32	22.81	23.18	23.57	24.05	24.47
26	26.15	28.08	26.38	26.96	27.40	27.87	28.44	28.92
30	30.17	32.38	30.43	31.09	31.60	32.13	32.78	33.34
34	34.19	36.71	34.46	35.21	35.78	36.37	37.09	37.73
38	38.23	41.06	38.53	39.38	40.01	40.69	41.50	42.22
42	42.25	45.39	42.57	43.50	44.19	44.93	45.82	46.61
46	46.27	49.71	46.62	47.64	48.40	49.20	50.17	51.02
50	50.29	54.01	50.65	51.75	52.57	53.43	54.46	55.39